Shot-Noise Detection in a Carbon Nanotube Quantum Dot

E. Onac,[1,*] F. Balestro,[1,†] B. Trauzettel,[1,2] C. F. J. Lodewijk,[1] and L. P. Kouwenhoven[1]

[1]*Kavli Institute of Nanoscience, Delft University of Technology, P.O. Box 5046, 2600 GA Delft, The Netherlands*

[2]*Instituut-Lorentz, Universiteit Leiden, P.O. Box 9506, 2300 RA Leiden, The Netherlands*

(Received 14 July 2005; published 19 January 2006)

An on-chip detection scheme for high frequency signals is used to detect noise generated by a quantum dot formed in a single wall carbon nanotube. The noise detection is based on photon assisted tunneling in a superconductor-insulator-superconductor junction. Measurements of shot noise over a full Coulomb diamond are reported with excited states and inelastic cotunneling clearly resolved. Super-Poissonian noise is detected in the case of inelastic cotunneling.

DOI: 10.1103/PhysRevLett.96.026803 PACS numbers: 73.63.Kv, 73.23.Hk, 73.63.Fg, 74.40.+k

The study of shot noise, i.e., nonequilibrium current fluctuations due to the discreteness of charge carriers, is an important tool for studying correlations induced in mesoscopic transport by different types of interactions [1,2]. Current is characterized by Poissonian shot noise when transport is determined by an uncorrelated stochastic process. Electron-electron interactions, such as Coulomb repulsion or resulting from the Pauli exclusion principle, can correlate electron motion and suppress shot noise. The noise power density is defined as the Fourier transform of the current-current correlator $S_I(\omega) = \int_{-\infty}^{+\infty} d\tau e^{i\omega\tau}\langle\delta I(t+\tau)\delta I(t)\rangle$. This definition is valid for both positive and negative frequencies ω, corresponding to energy absorption or emission by the device [3–5]. When $|eV| \gg |\hbar\omega|, k_BT$ (V is the voltage bias and T the temperature), shot noise dominates over other types of noise and the power density has a white spectrum that can be expressed as $S_I(-\omega) = S_I(\omega) = FeI$. Here I is the average current and the Fano factor F indicates the deviation from Poissonian shot noise for which $F = 1$. If the noise detector cannot distinguish between emission and absorption processes, a symmetrized version $S_I^{\text{symm}}(\omega) = S_I(\omega) + S_I(-\omega)$ is used. The Schottky formula $S_I^{\text{symm}} = 2eI$ refers to this symmetrized case.

For electron transport through a quantum dot (QD), shot noise can be either suppressed or enhanced with respect to the Poissonian value. First, for resonant tunneling, when a QD ground state is aligned between the Fermi levels in the leads, the Fano factor can vary between $1/2$ and 1. The exact value is determined by the ratio of tunneling rates between the dot and the two leads [6]. For strongly asymmetric barriers, transport is dominated by the most opaque one and shot noise is Poissonian. If the barriers are symmetric, the resonant charge state is occupied 50% of the time and a $F = 1/2$ shot-noise suppression is predicted. Second, when the QD is in Coulomb blockade, first-order sequential tunneling is energetically forbidden. Transport can still occur via cotunneling processes [7], elastic or inelastic. These are second-order processes, with a virtual intermediate state, allowing electron transfer between the leads. The elastic process leaves the QD in its ground state and transport is Poissonian. Inelastic cotunneling switches the system from a ground to an excited state and can lead to super-Poissonian noise with a Fano factor up to $F = 3$ [8]. Experiments have shown shot-noise suppression due to Coulomb blockade [9,10], but no experimental results exist on shot-noise enhancement in the inelastic cotunneling regime. Here we present the detection of noise, generated by a carbon nanotube quantum dot (CNT-QD). Excited states and inelastic cotunneling are clearly resolved in the noise measurements. For inelastic cotunneling, we find super-Poissonian shot noise.

We use an on-chip noise detector consisting of a superconductor-insulator-superconductor (SIS) junction. Noise generated in the CNT-QD leads to photon assisted tunneling between the superconducting electrodes of the SIS detector [see Figs. 1(a) and 1(b)]. This causes a change in the detector current, which contains information about the spectral power of noise [11]. The frequency range of the SIS detector is determined by the superconducting gap Δ (5–90 GHz for Al).

Sample fabrication necessitates five steps of e-beam lithography and material deposition for the different circuitry parts [12]. In intermediate steps, chemical vapor deposition [13] and atomic force microscope imaging are used for growing and locating the nanotubes. A 20 nm Pt layer is deposited for contacts and the lower plate of the coupling capacitances [see Fig. 1(b)]. For the insulating layer of the capacitances, we use 40 nm of SiO. In a last step, angle evaporation with an intermediary oxidation step is employed to deposit the Al tunnel junctions for the SIS detector and the upper plate of the capacitances.

Current fluctuations in the CNT-QD, $S_I(\omega)$, induce, via the coupling capacitances, voltage fluctuations across the detector, $S_V(\omega)$. The detector current in the absence of noise, $I_{\text{SIS},0}(V_{\text{det}})$, has a steplike shape [see Fig. 1(d)], which is modified by $S_V(\omega)$ into $I_{\text{SIS}}(V_{\text{det}})$. More specifically, the emission side of the spectrum $S_V(-\omega)$ induces a change $I_{\text{det}} = I_{\text{SIS}} - I_{\text{SIS},0}$ in the superconducting gap region ($0 < V_{\text{det}} < 2\Delta/e$) [12]:

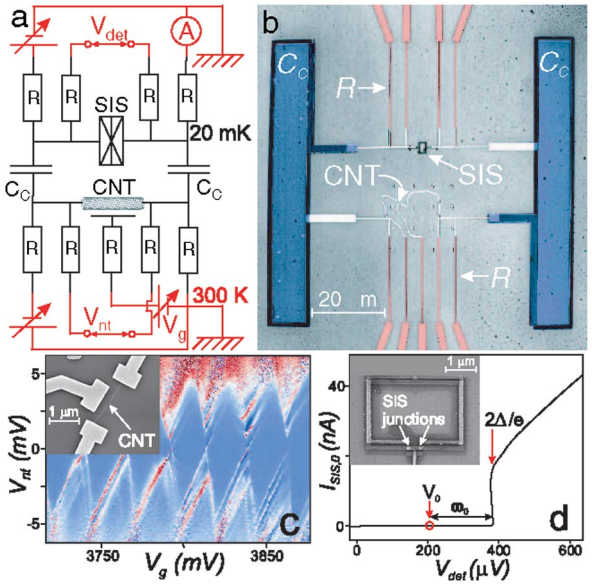

FIG. 1 (color). Schematic drawing of the circuit (a) and a scanning electron microscope (SEM) picture of the sample (b). The SIS detector is coupled, using two on-chip capacitances C_C (blue part), to the CNT-QD (the curly white lines are the custom made contacts) and is cooled to 20 mK. Four contact lines (red) are used for both the CNT and the detector. An additional contact on the CNT side is used as a side gate [see inset in (c)]. All lines incorporate an on-chip impedance R to prevent the high frequency signal from leaking via parasitic capacitances in the leads. These are thin Pt wires ($25 \times 0.1 \times 0.02$ μm) with a resistance between 2 and 2.25 kΩ, measured at 4 K. (c) Carbon nanotube dI_{nt}/dV_{nt} density plot shows standard Coulomb diamonds. Inset: SEM picture of the CNT with contacts and a side gate. (d) I-V characteristic of the detector SIS junction in the absence of noise. Current is zero in the superconducting gap region and is determined by the normal state resistance $R_N = 11.3$ kΩ for $V_{det} > 2\Delta/e$. Inset: SEM picture of the detector with two SIS junctions. This SQUID geometry allows us to suppress the supercurrent by means of an external magnetic field.

$$I_{det}(V_{det}) = \int_0^{+\infty} d\omega \left(\frac{e}{\hbar\omega}\right)^2 \frac{S_V(-\omega)}{2\pi} I_{SIS,0}\left(V_{det} + \frac{\hbar\omega}{e}\right). \quad (1)$$

Note that $I_{SIS,0}(V_{det}) \neq 0$ only for $V_{det} > 2\Delta/e$. If we consider a detector voltage $V_{det} = V_0$ [see example in Fig. 1(d)], then only frequencies above $\omega_0 = (2\Delta/e - V_0)/\hbar$ contribute to the detector current. This means that each point on the detector curve $I_{det}(V_0)$ represents noise detection over a bandwidth (ω_0, ∞). However, contributions from different frequencies are normalized as $S_V(\omega)/\omega^2$, leading to smaller changes in the detector current for higher frequencies. Finally, S_V is related to the CNT-QD current fluctuations by $S_V(-\omega) = S_I(-\omega)|Z(\omega)|^2$, with the transimpedance $Z(\omega)$ being determined by the coupling circuitry.

In the regime $|eV_{nt}| \gg |\hbar\omega|, k_BT$ (V_{nt} is the CNT bias voltage), shot noise dominates over other types of noise. Here the power density is proportional to the average current, $S_I \sim I$, and frequency independent $S_I(\omega) = S_I(-\omega) = S_I(0) = \text{const}$ (i.e., white spectrum). Equation (1) can then be written as:

$$I_{det}(V_{det}) = \frac{S_I(0)}{e} \kappa(Z, I_{SIS,0}, V_{det}), \quad (2)$$

with $\kappa = \int_0^{+\infty} d\omega [e^3/2\pi(\hbar\omega)^2] |Z(\omega)|^2 I_{SIS,0}(V_{det} + \frac{\hbar\omega}{e})$ a function that depends on transimpedance, detector I-V characteristic in the absence of noise, and detector bias. Equation (2) is valid, in general, for any white noise source that is coupled to the SIS detector junction.

The single wall carbon nanotube (CNT) has a length of 1.6 μm between the contacts and a side gate is used to change its electrical potential [see inset in Fig. 1(c)]. From the observation that we can induce both electron and hole transport at room temperature, we conclude that we have a small gap semiconductor CNT. After cooling to 20 mK, the conductance dI_{nt}/dV_{nt} density plot, as a function of applied bias V_{nt}, and gate voltage V_g show closing Coulomb diamonds, implying that one quantum dot is formed [see Fig. 1(c)]. Excited states are clearly stronger for one direction (parallel to one side of the Coulomb diamonds), indicating asymmetric tunnel barriers to the leads. From the size of the larger Coulomb diamonds, we estimate the addition energy $\delta + E_C \approx 4$ mV, with $\delta \approx 1$ meV the orbital energy and $E_C \approx 3$ meV the charging energy. The value for δ is consistent with the figure expected for a quantum dot formed by barriers at the contacts.

We fix the gate voltage at a Coulomb peak and current bias the nanotube. The detector signal I_{det}, presented as a function of the detector bias in Fig. 2, is increasing with the CNT current I_{nt}. The fact that the normalized curves I_{det}/I_{nt} are all identical, over this range of I_{nt} [see inset in Fig. 2(a)], proves that we are indeed measuring white shot noise. This is also apparent from the inset in Fig. 2(b), showing that the integrated detector signal depends linearly on the nanotube current.

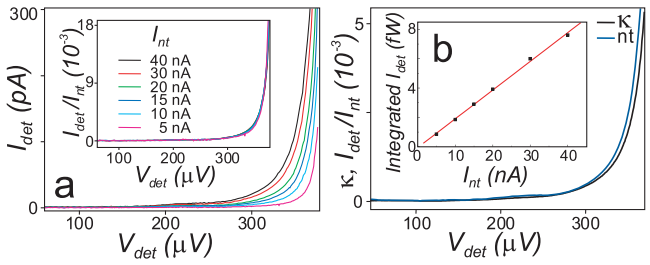

FIG. 2 (color). (a) Detector signal I_{det} as a function of detector bias V_{det} for several CNT current bias values I_{nt}. The maximum current bias $I_{nt} = 40$ nA corresponds to a voltage $V_{nt} = 11$ mV. Inset: Same detector curves normalized to CNT current. (b) Averages of normalized detector curves for the calibrating SIS-SIS, respectively, SIS-CNT sample. Inset: Integrated detector signal $\int I_{det} dV_{det}$ (for 140 μV $\leq V_{det} \leq$ 370 μV) versus CNT current I_{nt}.

Since the power spectral density can be expressed as $S_I = FeI_{nt}$, the normalized curve can be written as $I_{det}/I_{nt} = F\kappa(Z, I_{SIS,0}, V_{det})$. We determine the circuit calibration function κ by using a separate sample, in which well-known Poissonian noise is generated [11]. This calibration sample is fabricated simultaneously with the CNT sample but with an SIS junction as a noise source. The obtained calibration curve is presented in Fig. 2(b). We also plot there the normalized curve I_{det}/I_{nt}, averaged for CNT currents between 5 and 40 nA. The two curves have similar amplitudes, meaning that, for a given value of the current through the source, the detector signal is the same for the two samples. This indicates a Fano factor close to the Poissonian value $F = 1$ [14] for the high bias regime of the CNT. Based on these considerations, we use below the normalized curve $\kappa_{nt} = I_{det}/I_{nt}$, in Fig. 2(b) as a calibration curve. We estimate that the deviation of the Fano factor from the $F = 1$ value is less than 12% [12]. Our calibration allows for detection of changes in the Fano factor within this error bar.

We now focus on the two adjacent Coulomb diamonds in Fig. 3(a), with its derivative plotted in Fig. 3(b). Subsequently, we use the SIS detector to measure shot noise. We fix the gate voltage V_g and measure the detector current with finite (I_{SIS}) and zero ($I_{SIS,0}$) nanotube bias voltage V_{nt}. Then the values for V_g and V_{nt} are changed and the noise measurements repeated. In this way, we obtain the detector signal $I_{det} = I_{SIS} - I_{SIS,0}$ over the entire range of the Coulomb diamond.

For the noise detection, we sweep the V_{det} bias only over a limited interval (V^i_{det}, V^f_{det}) of the superconducting gap region, where the detector is most sensitive [15]. We obtain the noise power over this interval from

$$S_I/e = \int_{V^i_{det}}^{V^f_{det}} I_{det}(V_{det})dV_{det} \Big/ \int_{V^i_{det}}^{V^f_{det}} \kappa_{nt} dV_{det}. \qquad (3)$$

The resulting density plots for noise [see Figs. 3(c) and 3(d)] are in good correspondence with the ones from the standard dc measurement [Figs. 3(a) and 3(b)]. This is expected, as changes in I_{nt} also give changes in $S_I \propto I_{nt}$. There is a small shift in gate voltage values between the noise and the dc measurement (due to the long measurement time for noise detection). Excited states, as well as inelastic cotunneling signal inside the Coulomb diamond, are clearly resolved for both types of measurements.

The density plot for the Fano factor can be obtained by dividing the plots in Figs. 3(a) and 3(c), after careful alignment to correct for small gate shifts. In this way, we get the Fano factor values for specific regions outlined by the dashed and dotted lines in Fig. 3(b). These values, presented in Fig. 4(a), indicate a noise suppression ($F < 1$) at the closing of the diamond (dashed part) and an enhancement of noise ($F > 1$) in the regime of inelastic cotunneling (dotted part). Fano factor curves are also individually determined and plotted in Fig. 4(b).

We first consider the situation when the QD is outside Coulomb blockade [left part of Fig. 4(a) and black curve in Fig. 4(b)]. For small biases, close to the diamond crossing, we find that noise is suppressed, $F < 1$. This indicates that transport is not dominated by a single barrier and reso-

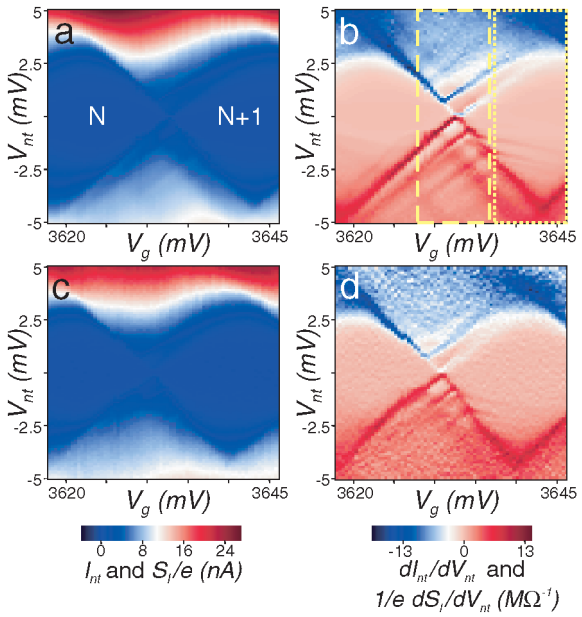

FIG. 3 (color). Density plots for dc [(a) and (b)] and noise measurements [(c) and (d)] as a function of nanotube bias V_{nt} and gate voltage V_g. Standard dc measurement of current I_{nt} and conductance dI_{nt}/dV_{nt} are presented in (a) and (b) for two adjacent Coulomb diamonds. The diamonds correspond to a fixed number of electrons (N, respectively $N + 1$) on the quantum dot. Noise power S_I obtained according to Eq. (3), together with its derivative dS_I/dV_{nt}, are presented in (c), respectively (d). Both are normalized to the electron charge such that we can use the same color scale for dc and noise measurements.

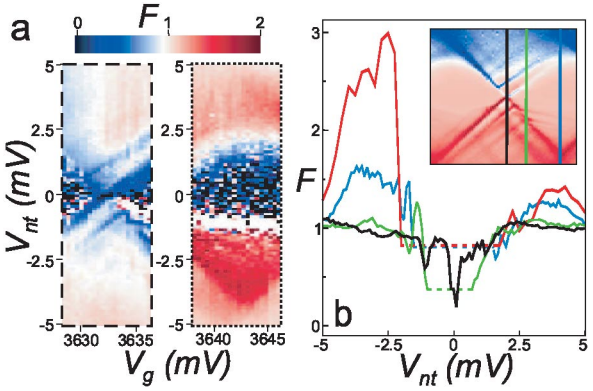

FIG. 4 (color). (a) Fano factor density plots corresponding to the two parts of the Coulomb diamond indicated in Fig. 3(b). (b) Individual Fano factor curves determined for gate voltages indicated in the inset density plot. The red curve was measured in a different Coulomb diamond. $F > 1$ indicates super-Poissonian noise corresponding to inelastic cotunneling. For CNT currents $I_{nt} < 150$ pA (the dashed part of the curves), no excess noise can be measured, with the sensitivity of our detection scheme.

nance effects matter. At large biases (where also $I_{nt} > 5$ nA), we detect Poissonian shot noise, in agreement with the calibration procedure. Thus, measurements in the sequential tunneling regime are consistent and prove that our detection scheme is reliable.

We now look at the region inside the Coulomb diamond, where transport occurs via cotunneling [see right part of Fig. 4(a)]. First, for elastic cotunneling, no noise is measured ($F \approx 0$ in the dark-blue region). This is a second-order process, in which an electron is transferred between the leads, via an intermediate virtual state. The electron has a very short dwell time and leaves the dot in its ground state. Subsequent elastic cotunneling events are completely uncorrelated and Poissonian shot noise is predicted, i.e., $F = 1$. However, our signal is obtained after subtracting the detector I-V in the absence of device bias: $I_{det} = I_{SIS} - I_{SIS,0}$, and, therefore, we measure only the excess noise (the noise induced by the CNT bias). In the regime of elastic cotunneling, I_{nt} is too small (<150 pA) to give a measurable contribution to the excess noise, and our substraction procedure yields $F \approx 0$.

Finally, we consider the inelastic cotunneling regime. The green curve in Fig. 4(b), taken at a gate value where inelastic cotunneling sets in, shows a small region in V_{nt} with super-Poissonian noise. The blue curve indicates an increase of the region with $F > 1$. Measurements of super-Poissonian noise, due to inelastic cotunneling, were also performed for other Coulomb diamonds [see red curve in Fig. 4(b)], showing a very pronounced Fano factor enhancement. Super-Poissonian noise can occur when two channels, with different transparencies, are available for transport [8,16]. If only one can be open at a time, electrons are transferred in bunches whenever transport takes place through the more transparent channel. Such conditions are met by a quantum dot in the inelastic cotunneling regime. In the ground state, current is blocked due to Coulomb interaction. Still, if the bias is larger than splitting between the ground and the first excited state, a second-order, inelastic tunneling process can take place and an electron is transferred from one lead to the other. The inelastic cotunneling leaves the dot in the excited state. The electron can subsequently either tunnel out or relax to the ground state and again block the current. Thus, depending on the tunneling rate through the excited state and the relaxation rate, we can distinguish two regimes. If the electron relaxes to the ground state, we are in the weak cotunneling regime. For noise, this is equivalent to elastic cotunneling (the electron always relaxes and tunnels out from the ground state) and leads to Poissonian noise $F = 1$. If relaxation is slow and transport takes place through the excited state (strong cotunneling regime), electrons are transferred in bunches and the noise becomes super-Poissonian. For inelastic cotunneling we measure $F > 1$, showing that we are in the strong cotunneling regime. Still, relaxation processes play an important role and lead to a Fano factor smaller than the maximum $F = 3$ predicted value.

Noise measurement over the entire Coulomb diamond region of a QD is reported for the first time. Features present in the standard current measurements, including excited states and inelastic cotunneling, are clearly resolved in noise measurements. This confirms the high sensitivity and versatility of our detection scheme. Super-Poissonian noise ($F > 1$), corresponding to inelastic cotunneling, is detected, also for the first time.

We are grateful to P. Jarillo-Herrero for assistance in the CNT fabrication. We acknowledge technical support from R. Schouten and B. van der Enden. Financial support was provided by the Dutch Organisation for Fundamental Research (FOM).

*Electronic address: eugen.onac@philips.com
†Present address: Laboratoire Louis Néel, associé au CNRS, BP 166, F-38042 Grenoble Cedex 9, France.

[1] Y. M. Blanter and M. Büttiker, Phys. Rep. **336**, 1 (2000).
[2] *Quantum Noise in Mesoscopic Physics*, edited by Y. V. Nazarov (Kluwer, Dordrecht, 2003).
[3] U. Gavish, Y. Levinson, and Y. Imry, Phys. Rev. B **62**, R10 637 (2000).
[4] R. Aguado and L. P. Kouwenhoven, Phys. Rev. Lett. **84**, 1986 (2000).
[5] R. J. Schoelkopf *et al.*, in Ref. [2].
[6] J. H. Davies, P. Hyldgaard, S. Hershfield, and J. W. Wilkins, Phys. Rev. B **46**, 9620 (1992).
[7] S. De Franceschi *et al.*, Phys. Rev. Lett. **86**, 878 (2001).
[8] E. V. Sukhorukov, G. Burkard, and D. Loss, Phys. Rev. B **63**, 125315 (2001); A. Thielmann, M. H. Hettler, J. König, and G. Schön, Phys. Rev. B **71**, 045341 (2005); Phys. Rev. Lett. **95**, 146806 (2005); W. Belzig, Phys. Rev. B **71**, 161301(R) (2005).
[9] H. Birk, M. J. M. de Jong, and C. Schönenberger, Phys. Rev. Lett. **75**, 1610 (1995).
[10] A. Nauen *et al.*, Phys. Rev. B **66**, 161303(R) (2002); **70**, 033305 (2004).
[11] R. Deblock, E. Onac, L. Gurevich, and L. P. Kouwenhoven, Science **301**, 203 (2003).
[12] E. Onac, Ph.D. thesis, TU Delft, 2005.
[13] J. Kong *et al.*, Nature (London) **395**, 878 (1998).
[14] A higher curve for the CNT sample is in agreement with a larger CNT impedance $R_S = 200\ \mathrm{k}\Omega$ compared with $R_N = 15\ \mathrm{k}\Omega$ of the SIS junction used for calibration [12].
[15] The applied detector bias is between 350 and 400 μV. Because of series resistances in the circuit, this results in a real detector bias between $V^i_{det} \simeq 333\ \mu$V and $V^f_{det} \simeq 370\ \mu$V. The corresponding cutoff frequencies $\omega_i \simeq 13.2$ GHz and $\omega_f \simeq 4.3$ GHz represent the lower limit for the detection bandwidth.
[16] S. S. Safonov *et al.*, Phys. Rev. Lett. **91**, 136801 (2003).